ANALYSIS OF NITROGEN AND STEAM INJECTION IN A POROUS MEDIUM WITH WATER

J. BRUINING AND D. MARCHESIN

ABSTRACT. We formulate conservation laws governing steam and nitrogen injection in a one-dimensional porous medium containing water. Compressibility, heat conductivity and capillarity are neglected. We study the condensation front and shock waves arising in the flow.

We find that there are four possible types of solutions for the initial and boundary conditions of interest. We describe a simple construction in the temperature saturation plane that determines the complete solution for the given conditions.

Applications of the theory developed here are in clean up of soil contaminated with non-aqueous phase liquids. We show that a substantial cold gaseous zone develops in all solutions of practical interest, thus counteracting downward migration of the pollutant.

1. INTRODUCTION

The continuing widespread occurrence of contamination due to spills and leaks of organic materials such as petroleum products which occur during their transport, storage and disposal causes problems for our high-quality ground-water resources. In spite of increased awareness of the environmental impacts of oil spills it appears to be impossible to avoid these accidents. Organic pollutants are referred to as non-aqueous phase liquids (NAPL), which may have a density smaller than water (LNAPL) or larger than water (DNAPL). Traditional clean up methods of these spills such as pump-and-treat are slow because diffusion/dissolution are the main removal mechanisms. Long clean up times particularly occur for highly heterogeneous conditions [13],[23].

Removal of contaminants with steam is an alternative. Steam injection is widely studied in Petroleum Engineering [33],[31], [12]. Steam injection leads to an expanding heated zone, separated from the original cold zone by a short transition zone, where most of the steam condenses. The transition zone is often considered as a front, the so-called steam condensation front. Steam can also clean parts that are indirectly heated by conduction. Therefore the effect of heterogeneity is smaller because the conductivity is much less heterogeneous than the permeability. Consequently steam is able to recover organic pollutants from highly impermeable parts and is able to reduce the amount of oil left to virtually zero. None of the other techniques known today is able to compete with these two advantages of steam. There is an abundant literature on experimental [15] and theoretical [14] modeling of steam injection for clean up and oil recovery.

Key words and phrases. Steam injection, thermal recovery, porous media, multiphase flow, hyperbolic systems, bifurcation.

This work was supported in part by: CNPq under Grant 301532/2003-6, FINEP under CTPETRO Grant 21.01.0248.00, MCT under Grant PCI 170.676/2003-0, Brazil; NWO under Fellowship Grant R 75-389, The Netherlands; IMA (Univ. of Minnesota), Dietz Laboratory (TU Delft, The Netherlands), IMPA (Brazil). Support of the steam recovery research work by Delft University of Technology and by Shell is also acknowledged as well as by the Inst. Milenio-AGIMB and IMPA.

There are, however, a number of problems with steam that are still not optimally solved. One problem is that steam at normal boiling temperatures completely destroys the ecosystem. Another is the downward migration of DNAPL as it accumulates near the steam condensation front [2], b[25]. In both cases simultaneous injection of steam with nitrogen or air is able to alleviate the problem. Simultaneous injection of a non-reactive gas lowers the temperature of the steam at a given total pressure, because the water pressure becomes lower. A lower water pressure leads to a lower boiling point. Therefore less energy is required to heat up the soil to a lower temperature. The important feature that leads to a reduction of downward movement is the possible formation of a cold gaseous zone downstream of the steam condensation front. Such a gaseous zone does not occur when pure steam is injected. The mechanism that counteracts downward displacement is that the condensing NAPL's are spread out in the gaseous zone, which reduces its relative permeability and hence the rate at which it moves downward. This mechanism has been investigated both theoretically and experimentally [16], [24]. However, it has not been investigated whether a downstream cold gaseous zone will always exist for all possible conditions. The existence of such a zone is a prerequisite to counteract downward movement. In the same way there can be conditions such that a downstream cold gaseous zone exists, but it is very short. It is also important to know that optimal conditions to counteract downward movement can be maintained even after heat loss effects.

In order to investigate whether a sufficiently large cold gaseous zone will be present for all possible conditions it is useful to obtain a complete set of solutions for a representative system of model equations. Such a representative system can consist of the component mass balance equations and the energy balance equation supplemented with Darcy's law of multi-phase flow. For a distribution of components among the phases we may assume thermodynamic equilibrium. In a 1-D setting, diffusional processes such as molecular diffusion, dispersion, thermal conduction and capillary effects are usually small and can be disregarded. Therefore the model equations only contain an accumulation term and a convection term. We will refer to the model equations with only accumulation and convection terms as equations in the hyperbolic framework.

By a complete set of solutions we understand all types of solutions that are qualitatively different. A well known example of solutions that are qualitatively different for steam injection in oil reservoirs is presented in the classical paper by Mandl and Volek [18], who show that below a critical (non-zero) steam quality the steam condensation front ceases to exist and a steam drive is converted to a hot water drive.

Recent developments in the theory of bifurcations occurring in systems of hyperbolic conservation equations have led to a methodology to find all qualitatively different solutions. A review of the theory is summarized for a petroleum engineering audience in an appendix of [19]. In order to keep the problem tractable we consider steam-nitrogen flow in the fully saturated zone and ignore the presence of the NAPL contaminant. We leave this for future work. The solutions of the steam-nitrogen flow problem can be conveniently illustrated graphically in the temperature, water saturation (T, S_w) space. In this phase diagram all types of solutions can be shown and bifurcation conditions are curves in this space. These curves are loci where wave speeds become equal or attain maximum values. Whenever a solution path crosses such a bifurcation curve a new type of solution is expected. Because many model parameters are fixed e.g. the temperature dependence of the densities and viscosities and other parameters such as porosity and residual saturations show only small

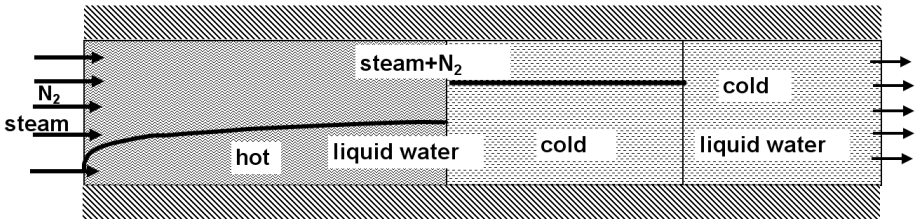

FIGURE 2.1. Schematic representation of one of the possible saturation and temperature profiles during steam/nitrogen injection in an originally water filled core.

variations the topological structure of the phase diagram is in this case representative for all conditions. Indeed even various expressions of relative permeabilities will lead to the same type of diagram.

In Section 2 we will describe the model for steam-nitrogen injection. We will formulate the equations in the hyperbolic frame work. We will prove some important properties of the solution of the equations. In Section 3 we will formulate the Hugoniot conditions at the steam condensation front. In Section 4 we discuss the rarefactions and shocks away from condensation. In Section 5 we determine the structure of the Riemann solutions and in Section 6 we show the phase diagrams of a solution for an initially water saturated core. Appendix A contains a table explaining all the symbols. Moreover Appendix A summarizes all relevant dependencies of physical properties on temperature. Some calculations relevant for the main change in wave sequence appear in Appendix B.

2. The model for water displacement by mixed steam air injection

2.1. **Physical considerations.** We consider the injection of water, steam, and nitrogen or other non-reactive gas in a linear core originally filled with water (see Fig. 2.1). The core consists of sand with constant porosity φ and permeability k. The core is horizontal and we disregard the effects of gravity. Transverse capillary pressure diffusion is sufficiently large to guarantee a uniform saturation over the cross-section. The displacement is considered to occur at constant pressure, in the sense that we disregard any effect on the thermodynamic properties or fluid viscosities due to flow induced pressure variations.

In the core we find two wide regions viz. a hot region and a cold region as well as a short steam condensation zone, which we call steam condensation front. Regions are further subdivided into zones according to the phases present. In each of the regions there can be two-phase or single phase flow. We will assume local thermodynamic equilibrium in each of the wide regions. This means that in the two-phase zones the temperature is determined by the partial pressure of the steam and is given by an empirical relation. Non-equilibrium effects can occur in the transition zones between the wide regions, but an explicit mathematical description of the transition zone can be avoided in the current treatment. If a superheated gaseous mixture were injected at the beginning of the hot zone, this beginning zone would be of a single phase region. The temperature in the the hot zone will lie below the injection temperature. The cold zone will be at the original reservoir temperature.

In two-phase flow regions the gaseous phase consists of nitrogen and steam, whereas the liquid phase consists only of water. The gases exhibit ideal behavior. Consequently we disregard any heat of mixing effect between the gases and assume that the volumes of the gases are additive, i.e., there is no volume contraction effect upon mixing. We disregard any dissolution of nitrogen in the water. We assume that the viscosity of the gaseous phase is independent of composition, but we take the gaseous phase temperature dependence into account. The liquid water viscosity depends only on the temperature and we describe it by a correlation for pure water viscosity. In the two-phase regions we apply Darcy's law for multiphase flow. We use power law relative permeabilities. Capillary forces are ignored. The density of water depends on temperature, but it is independent of the total pressure.

In the single phase zones only water flows. The water has the same properties as described above for the two-phase region.

2.2. **The mass balance evolution equations.** The conservation of mass of each component in each phase is given by the following equations, which express liquid water mass balance, steam mass balance in the gaseous phase, and nitrogen mass conservation in the gaseous phase (see for notation [8]):

$$\begin{aligned}
&\frac{\partial}{\partial t}(\varphi \rho_W S_w) + \frac{\partial}{\partial x}(\rho_W u_w) = q_{g\to a,w},\\
&\frac{\partial}{\partial t}(\varphi \rho_{gw} S_g) + \frac{\partial}{\partial x}(\rho_{gw} u_{gw}) = -q_{g\to a,w},\\
&\frac{\partial}{\partial t}(\varphi \rho_{gn} S_g) + \frac{\partial}{\partial x}(\rho_{gn} u_{gn}) = 0.
\end{aligned} \tag{2.1}$$

In these equations S_w is the water saturation, i.e., the fraction of the pores filled with water and S_g is the gas saturation. Furthermore u_w is the Darcy velocity of water, and $q_{g\to a,w}$ is the condensation rate. We use ρ_{gw} to denote the concentration of steam in the gaseous phase, i.e., the mass of steam per unit volume. In the same way we define the concentration of nitrogen ρ_{gn}. We also define the flow rate of steam as u_{gw}. This flow rate consists of a contribution due to the Darcy velocity of the gas u_g and a contribution due to diffusion. The flow rate of nitrogen is given as u_{gn}, and it also consists of a contribution due to the Darcy velocity and a contribution due to diffusion. This diffusion contribution is ignored here as it will be further elaborated in another paper. Hence it is assumed that $u_{gw} = u_{gn} = u_g$ is the volume averaged Darcy velocity.

2.2.1. *Fractional flow formulation.* Darcy's law of multiphase flow relates pressure gradient in a fluid with its Darcy velocity ([9]):

$$u_w = -\lambda_w \frac{\partial p_w}{\partial x}, \quad u_g = -\lambda_g \frac{\partial p_g}{\partial x},$$

where the water and gas mobilities are $\lambda_w = k k_{rw}/\mu_w$ and $\lambda_g = k k_{rg}/\mu_g$.

If capillary pressure is neglected, the pressure difference between p_w and p_g can be ignored. In this case the flow functions f_w, f_g denote the fractional flows and are defined by ([9]):

$$f_w = \frac{\lambda_w}{\lambda_w + \lambda_g} \quad \text{and} \quad f_g = \frac{\lambda_g}{\lambda_w + \lambda_g}; \tag{2.2}$$

thus the Darcy velocities are

$$u_w = u f_w, \quad u_g = u f_g, \tag{2.3}$$

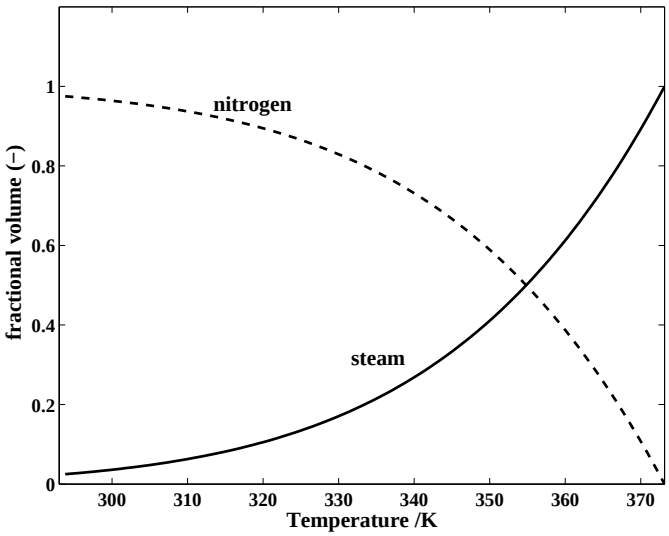

FIGURE 2.2. Fractional volumes of steam ψ_{gw} and nitrogen ψ_{gn} as functions of temperature. The convexity of the curves is such that condensation will occur in shocks rather than in rarefactions.

where

$$u = u_w + u_g \tag{2.4}$$

is the total Darcy velocity. Eqs. (2.1) become

$$\frac{\partial}{\partial t}\left(\varphi \rho_W S_w\right) + \frac{\partial}{\partial x}\left(u \rho_W f_w\right) = q_{g\to a,w}, \tag{2.5}$$

$$\frac{\partial}{\partial t}\left(\varphi \rho_{gw} S_g\right) + \frac{\partial}{\partial x}\left(u \rho_{gw} f_g\right) = -q_{g\to a,w}, \tag{2.6}$$

$$\frac{\partial}{\partial t}\left(\varphi \rho_{gn} S_g\right) + \frac{\partial}{\partial x}\left(u \rho_{gn} f_g\right) = 0. \tag{2.7}$$

2.2.2. *Physical properties of fluids.* Nitrogen and steam in the gaseous phase are assumed to behave as ideal gases. In particular the mass densities of these gases can be written as

$$\rho_{gW} = \frac{M_W p_{tot}}{RT}, \qquad \rho_{gN} = \frac{M_N p_{tot}}{RT}, \tag{2.8}$$

where M_W, M_N are the molecular weights of water and nitrogen respectively and R is the gas constant. The capital W and N as subscript of ρ emphasize that these are densities of the pure components. Since in ideal gas behavior assumed in this work, there are no volume effects due to mixing; similarly, the enthalpy changes due to mixing of the gas components are zero. Therefore the volumes of the components are additive:

$$\frac{\rho_{gw}}{\rho_{gW}} + \frac{\rho_{gn}}{\rho_{gN}} = 1. \tag{2.9}$$

Using Eq. (2.9), the concentration of steam ρ_{gw} and of nitrogen ρ_{gn} in the mixture can be expressed in terms of the pure phase densities ρ_{gW}, ρ_{gN} as

$$\rho_{gw} = \rho_{gW}\psi_{gw}, \quad \rho_{gn} = \rho_{gN}\psi_{gn}. \tag{2.10}$$

This equation can be regarded as defining the volume fractions ψ_{gw} and ψ_{gn} of steam and nitrogen in the gaseous phase. (See Fig. 2.2.) The entire two-phase thermodynamic behavior is specified by the equilibrium condition between water and steam given by Eq. (A.8) and the densities ρ_{gw}, ρ_{gN} are computed using (A.9).

All other properties relevant to the computation are summarized in Appendix A.

2.3. **The energy evolution equation.** The conservation of enthalpy is given as

$$\frac{\partial}{\partial t}\big(H_r + \varphi S_w \rho_W h_W + \varphi S_g \left(\rho_{gw} h_{gW} + \rho_{gn} h_{gN}\right)\big) + \frac{\partial}{\partial x}\big(u_w \rho_W h_W + u_g \left(\rho_{gw} h_{gW} + \rho_{gn} h_{gN}\right)\big) = 0. \tag{2.11}$$

The basis of using this equation can be found in [3] (page 323, Table 10.4-1, Eq. R) and [1] page 144, footnote). It uses the assumption (see section 2.1) that as to the thermodynamic quantities the system is at constant pressure. Upscaling issues regarding the equations in porous media can be found in [20].

The enthalpies h are all per unit mass and depend on temperature and pressure (see Appendix A). The enthalpy of water in the gaseous phase is h_{gW}, and h_W is the enthalpy of water in the liquid aqueous phase while h_{gN} is the enthalpy of nitrogen in the gaseous phase. In Equation (2.11) thermal conductivity has been disregarded, as we are in the hyperbolic framework.

Remark 2.1. The volume fractions $\psi_{gw} = \rho_{gw}/\rho_{gW}$ and $\psi_{gn} = \rho_{gn}/\rho_{gN}$ add up to one (see Equation (2.9)) so that the four equations (2.5)–(2.7), (2.11) carry four unknowns, namely, the condensation rate $q_{g\to a,w}$, the water saturation S_w, the temperature T, and the total velocity u. Clearly we have $S_g = 1 - S_w$, and $\rho_{gw} = \rho_{gw}(T)$, $\rho_{gn} = \rho_{gn}(T)$ for a given total pressure p_{tot}.

2.3.1. *Sensible and latent parts of steam enthalpy.* In Eq. (2.11), we split the enthalpy of steam h_{gW} into a sensible part h^s_{gW} and a latent part $\bar{\Lambda}$ evaluated at the reference temperature $\bar{T}$:

$$h_{gW} = h^s_{gW} + \bar{\Lambda}. \tag{2.12}$$

We substitute Eq. (2.12) into Eq. (2.11). The terms that contain the factor $\bar{\Lambda}$ in the resulting equation are:

$$\bar{\Lambda}\left(\frac{\partial}{\partial t}\left(\varphi S_g \rho_{gw}\right) + \frac{\partial}{\partial x}(u_g \rho_{gw})\right) = \bar{\Lambda} q_{g\to a,w},$$

where we have used the steam balance Equation (2.6) to obtain the right hand side of this equation. Hence Eq. (2.11) can be rewritten as the final equation

$$\frac{\partial}{\partial t}\left(H_r + \varphi S_w H_W + \varphi S_g \left(H^s_{gw} + H_{gn}\right)\right) + \frac{\partial}{\partial x}(u_w H_W + u_g \left(H^s_{gw} + H_{gn}\right)) = \bar{\Lambda} q_{g\to a,w}. \tag{2.13}$$

2.3.2. *The condensation rate equation.* The precise form of $q_{g\to a,w}$ is not required in the hyperbolic framework. In this context, it suffices to know that the condensation rate $q_{g\to a,w}$ is a nonnegative quantity that vanishes outside the region spanned by the SCF.

The quantity $\bar{\Lambda}$ in (2.13) represents the heat required to obtain steam at temperature T from liquid water at reference temperature $\bar{T}$ and hence it is positive below the critical

pressure. It can be shown that for two-phase flow the temperature is constant precisely where $q_{g\to a,w} = 0$ identically.

2.4. **The equations in the hyperbolic framework.** The equations in hyperbolic framework disregard diffusion, capillary terms, as well as heat conductivity. They are appropriate for the study of rarefaction waves as well as for the condensation and shock waves for shock waves and for condensation waves [32]. From Eqs. (2.5)–(2.7), we obtain

$$\frac{\partial}{\partial t}\left(\varphi\rho_W S_w\right) + \frac{\partial}{\partial x}\left(u\rho_W f_w\right) = \frac{\partial Q}{\partial x}, \tag{2.14}$$

$$\frac{\partial}{\partial t}\left(\varphi\rho_{gw} S_g\right) + \frac{\partial}{\partial x}\left(u\rho_{gw} f_g\right) = -\frac{\partial Q}{\partial x}, \tag{2.15}$$

$$\frac{\partial}{\partial t}\left(\varphi\rho_{gn} S_g\right) + \frac{\partial}{\partial x}\left(u\rho_{gn} f_g\right) = 0, \tag{2.16}$$

where we have introduced cumulative condensation rate $Q(x,t)$ as

$$\frac{\partial Q}{\partial x}(x,t) = q_{g\to a,w}, \quad \text{such that} \quad Q(x\to-\infty,t) = 0. \tag{2.17}$$

From Eqs. (2.17) and (2.13) we obtain

$$\frac{\partial}{\partial t}(H_r + \varphi(H_W S_w + H_g^s S_g)) + \frac{\partial}{\partial x}\big(u(H_W f_w + H_g^s f_g)\big) = \bar{\Lambda}\frac{\partial Q}{\partial x}. \tag{2.18}$$

In the hyperbolic framework, the equations for steam and air injection are (2.14)–(2.18).

Remark 2.2. bBy manipulating Eq. (2.14)-(2.16) and (2.18), it can be shown that the thermal velocity for zero $q_{g\to a,w}$ is

$$\lambda_o^{TH} = u\frac{C_W f_w + C_g f_g}{C_r + \varphi(C_W S_w + C_g S_g)}. \tag{2.19}$$

In general for non-zero $q_{g\to a,w}$ the expression of λ^{TH} is different. We will find it useful to define $\tilde{\lambda}_o^{TH} = (\varphi/u)\lambda_o^{TH}$.

3. The Rankine-Hugoniot conditions for the steam condensation front

The Rankine-Hugoniot conditions are the mathematical expressions for a balance equation (e.g. mass balance or energy balance) at a shock i.e. position in space where we have a discontinuous change of variables (see Eq. 2.18 in reference [32]). An example is the shock in the Buckley-Leverett problem. The Rankine-Hugoniot conditions relate the state upstream and downstream of any shock (including the steam condensation front) with its speed.

3.1. **Formulation of the Rankine-Hugoniot conditions.** The Hugoniot equations at the steam condensation front are obtained from Eqs. (2.14)–(2.17). The velocity v^{SCF} is the velocity of the steam condensation front. Here $(+)$ denotes the state at right (downstream) of the shock, while $(-)$ denotes the state at the left (or upstream).

$$-\varphi v^{SCF}\left((\rho_W S_w)^+ - (\rho_W S_w)^-\right) + (u\rho_W f_w)^+ - (u\rho_W f_w)^- = Q^+, \tag{3.1}$$

$$-\varphi v^{SCF}\left((\rho_{gw} S_g)^+ - (\rho_{gw} S_g)^-\right) + (u\rho_{gw} f_g)^+ - (u\rho_{gw} f_g)^- = -Q^+, \tag{3.2}$$

$$-\varphi v^{SCF}\left((\rho_{gn} S_g)^+ - (\rho_{gn} S_g)^-\right) + (u\rho_{gn} f_g)^+ - (u\rho_{gn} f_g)^- = 0. \tag{3.3}$$

In Eqs. (3.1) and (3.2) we have used the fact that $Q^- = 0$ by the definition in Eq. (2.17).

The Hugoniot condition for the energy is derived in the same way from Eq. (2.18):

$$- v^{SCF}\Big((H_r + \varphi(H_W S_w + H_g^s S_g))^+ - (H_r + \varphi(H_W S_w + H_g^s S_g))^-\Big)$$
$$+ \big(u(H_W f_w + H_g^s f_g)\big)^+ - \big(u(H_W f_w + H_g^s f_g)\big)^- = \bar{\Lambda} Q^+. \tag{3.4}$$

The four equations (3.1), (3.2), (3.3) and (3.4) are all linear in terms of u^+, Q^+, v^{SCF}. Therefore we choose three equations (two appropriate combinations of the mass balance equations and the energy equation) to obtain the values of u^+, Q^+, v^{SCF} in Section 3.2. Then in Section 3.3.1 we use the remaining mass balance equation as a non-linear equation for S_w^+.

Remark 3.1. Equation (3.4) can be simplified by the use of constant heat capacities:

$$-\varphi v^{SCF}\big(C_r/\varphi + C_W S_w^- + C_g^- S_g^-\big) + u^-\big(C_W f_w^- + C_g^- f_g^-\big) - \Lambda_c^+ Q^+ / \big(T^+ - T^-\big) = 0, \tag{3.5}$$

where the abbreviation $\Lambda_c = \Lambda_c(T)$ is given by

$$\Lambda_c = \bar{\Lambda} + (c_{gW} - c_W)(T - \bar{T}). \tag{3.6}$$

Without loss of generality it can be assumed that H_w^+, H_g^{s+} are zero and H_w^-, H_g^{s-} are enthalpies with respect to T^+.

The term Λ_c approximates the heat required to convert liquid water at temperature T to steam at the same temperature. It is a positive quantity (see the following remark).

Remark 3.2. We are only interested in temperatures T^+ and T^- below the critical temperature T_c i.e. the temperature at which the physical difference between the liquid and its vapor ceases to exist. Below the critical temperature the heat of evaporation $\Lambda(T) = (\bar{\Lambda} + h_{gW}^s - h_W)$ is positive, while at the critical point it vanishes: $\Lambda(T_c) = 0$, and $v^{SCF} = \lambda_o^{TH}(-) = \lambda_o^{TH}(+)$, i.e., the speed of the steam condensation front, the thermal characteristic speeds at the left and right become equal. Taking the limits $T^+ - T^- \to 0$ with $T^+ < T^- < T_c$ in Eq. (3.4), that is the same as in Eq. (3.5), $Q^+ \to 0$ and we observe that for subcritical temperatures $\lambda_o^{TH}(-) \le \lambda^{TH}(-)$ and $\lambda_o^{TH}(+) \le \lambda^{TH}(+)$. Here λ^{TH} is defined as

$$\lambda^{TH}(T) = \lim_{T^+, T^- \to T} v^{SCF}. \tag{3.7}$$

Remark 3.3. Sometimes it is useful to consider all possible solutions (T^+, S_w^+, u^+) of the Rankine-Hugoniot conditions for a fixed left state (T^-, S_w^-, u^-) when the shock speed varies. This is a one parameter family of points in the temperature-saturation-velocity space, which is called the Hugoniot curve for (T^-, S_w^-, u^-). One of its main features is that it determines between which waves the shock exists. Another feature is that it determines conditions for which the generic features of a solution changes i.e. when bifurcations occur.[19].

3.2. **Independence of the secondary variables on S_w^+.** Assume that we are given values for T^-, S_w^- and T^+. In the solution of the equations (3.1), (3.2), (3.3) and (3.4) for a steam condensation front, we will show that the secondary variables v^{SCF}, u^+, Q^+ are determined independently of the value of S_w^+. To do so, we divide equations (3.1), (3.2) and (3.3) by u^-, and introduce

$$\tilde{v}^{SCF} := \frac{\varphi v^{SCF}}{u^-}, \quad \tilde{u}^+ := \frac{u^+}{u^-}, \quad \tilde{Q}^+ := \frac{Q^+}{u^-}. \tag{3.8}$$

Note that $\rho_{gn}^{+}=0$ at the normal boiling temperature of water.

Dividing each of the resulting equation by the corresponding density ρ_W^+ and concentrations ρ_{gw}^+, ρ_{gn}^+, we obtain:

$$-\left(S_w^+-\frac{\rho_W^-}{\rho_W^+}S_w^-\right)\tilde{v}^{SCF}+f_w^+\tilde{u}^+-\frac{\tilde{Q}^+}{\rho_W^+}=\frac{\rho_W^-}{\rho_W^+}f_w^-, \tag{3.9}$$

$$-\left(S_g^+-\frac{\rho_{gw}^-}{\rho_{gw}^+}S_g^-\right)\tilde{v}^{SCF}+f_g^+\tilde{u}^+-\frac{\tilde{Q}^+}{\rho_{gw}^+}=\frac{\rho_{gw}^-}{\rho_{gw}^+}f_g^-, \tag{3.10}$$

$$-\left(S_g^+-\frac{\rho_{gn}^-}{\rho_{gn}^+}S_g^-\right)\tilde{v}^{SCF}+f_g^+\tilde{u}^+=\frac{\rho_{gn}^-}{\rho_{gn}^+}f_g^-. \tag{3.11}$$

We add equations (3.9) and (3.10), as well as (3.9) and (3.11), obtaining:

$$\left(-1+\frac{\rho_W^-}{\rho_W^+}S_w^-+\frac{\rho_{gw}^-}{\rho_{gw}^+}S_g^-\right)\tilde{v}^{SCF}+\tilde{u}^+-\left(\frac{1}{\rho_{gw}^+}-\frac{1}{\rho_W^+}\right)\tilde{Q}^+=\frac{\rho_W^-}{\rho_W^+}f_w^-+\frac{\rho_{gw}^-}{\rho_{gw}^+}f_g^-, \tag{3.12}$$

$$\left(-1+\frac{\rho_W^-}{\rho_W^+}S_w^-+\frac{\rho_{gn}^-}{\rho_{gn}^+}S_g^-\right)\tilde{v}^{SCF}+\tilde{u}^+-\frac{1}{\rho_W^+}\tilde{Q}^+=\frac{\rho_W^-}{\rho_W^+}f_w^-+\frac{\rho_{gn}^-}{\rho_{gn}^+}f_g^-. \tag{3.13}$$

We supplement the two linearly independent equations above by the following rewritten version of the energy conservation equation (3.4). We multiply Eqs. (3.1), (3.2), (3.3) by their respective enthalpies h_W^+, h_{gW}^{s+}, h_{gN}^+, and subtract from Eq. (3.4), obtaining

$$\Delta H_m^{-,+}\tilde{v}^{SCF}-\Lambda^+\widetilde{Q}^+=\Delta J_H^{-,+}, \tag{3.14}$$

where the heat of evaporation Λ^+ at temperature T^+ is defined by

$$\Lambda^+=\bar{\Lambda}+h_{gW}^{s+}-h_W^+. \tag{3.15}$$

and we abbreviated the enthalpy content of the medium $\Delta H_m^{-,+}$, the enthalpy flux $\Delta J_H^{-,+}$ as follows:

$$\begin{aligned}\Delta H_m^{-,+}&:=(H_r^--H_r^+)/\varphi+\rho_W^-(h_W^--h_W^+)S_w^-+\left(\rho_{gw}^-(h_{gW}^{s-}-h_{gW}^{s+})+\rho_{gn}^-(h_{gN}^--h_{gN}^+)\right)S_g^-,\\ \Delta J_H^{-,+}&:=\rho_W^-(h_W^--h_W^+)f_w^-+\left(\rho_{gw}^-(h_{gW}^{s-}-h_{gW}^{s+})+\rho_{gn}^-(h_{gN}^--h_{gN}^+)\right)f_g^-.\end{aligned} \tag{3.16}$$

Eqs. (3.12), (3.13) and (3.14) are a linear system in three variables $\tilde{v}^{SCF}$, $\tilde{u}^+$, $\tilde{Q}^+$, with coefficients and right hand side that do not depend on S_w^+. Therefore these variables do not depend on S_w^+.

Remark 3.4. One consequence of the calculation in this Section is that we can consider T, S_w as primary variables and $\tilde{v}^{SCF}$, $\tilde{u}^+$, $\tilde{Q}^+$ as secondary variables. That is, we study the Rankine-Hugoniot relations for (T^+,S_w^+), (T^-,S_w^-) in the (T,S_w) plane without worrying about the secondary variables; the latter are computed at the end of the calculation.

3.3. **Condensation solution of the Rankine-Hugoniot system.** We are given values for T^-,S_w^- and T^+. Now we solve Eqs. (3.12), (3.13) and (3.14) as a linear system in the three variables $\tilde{v}^{SCF}$, $\tilde{u}^+$, $\tilde{Q}^+$. Subtracting (3.12) from (3.13) we obtain after reordering:

$$\left(\frac{\rho_{gw}^-}{\rho_{gw}^+}-\frac{\rho_{gn}^-}{\rho_{gn}^+}\right)S_g^-\,\tilde{v}^{SCF}+\frac{1}{\rho_{gw}^+}\tilde{Q}^+=\left(\frac{\rho_{gw}^-}{\rho_{gw}^+}-\frac{\rho_{gn}^-}{\rho_{gn}^+}\right)f_g^-. \tag{3.17}$$

We use Eq. (3.17) to extract $\tilde{Q}^+$ and substitute in equation (3.14) obtaining

$$\left(\frac{\Delta H_m^{-,+}}{\Lambda^+} + \rho_{gw}^+\left(\frac{\rho_{gw}^-}{\rho_{gw}^+} - \frac{\rho_{gn}^-}{\rho_{gn}^+}\right) S_g^-\right)\tilde{v}^{SCF} = \rho_{gw}^+\left(\frac{\rho_{gw}^-}{\rho_{gw}^+} - \frac{\rho_{gn}^-}{\rho_{gn}^+}\right) f_g^- + \frac{\Delta J_H^{-,+}}{\Lambda^+}. \tag{3.18}$$

Notice that for $T^+ = T^-$ the coefficient of $\tilde{v}^{SCF}$ is zero, so the solution described in this Section 3.3 is only valid for $T^+ \neq T^-$. In Appendix B we prove that the coefficients of $\tilde{v}^{SCF}$ in Eq. (3.18) and (3.17) are positive in our case, where $T^+ < T^-$.

The coefficient of $\tilde{v}^{SCF}$ in Eq. (3.18) is easily seen to be the determinant of the system (3.12)–(3.14). If this coefficient is assumed to be non-zero, $\tilde{v}^{SCF}$ is determined. Substitution into (3.17) provides the value of $\widetilde{Q}^+$. Finally we obtain from Eq. (3.13) the value of $\widetilde{u}^+$. Where the coefficient of $\tilde{v}^{SCF}$ is zero a bifurcation will occur (i.e. at $T^+ = T^-$). So away from the bifurcation the system can be solved uniquely.

3.3.1. *Calculation of S_w^+.* We have found the quantities $\tilde{v}^{SCF}$, $\tilde{u}^+$, $\tilde{Q}^+$. We divide Eq. (3.9) by $\tilde{u}^+$ and we rearrange, obtaining:

$$f_w(S_w^+) = \frac{\tilde{v}^{SCF}}{\tilde{u}^+} S_w^+ + \frac{\rho_W^- f_w^- + \tilde{Q}^+ - \rho_W^- S_w^- \tilde{v}^{SCF}}{\tilde{u}^+ \rho_W^+}. \tag{3.19}$$

The graph of the right hand side is a straight line in a S_w^+, f_w^+ plot, which has at most three intersections with the graph of $f_w(S_w^+)$. Each intersection of the two graphs is a point in the Hugoniot curve in the (T^+, S_w^+) plane. As T^+ varies each intersection generates a part of the Hugoniot curve. Tangency of the two graphs makes two parts coalesce: the number of intersections changes by two, originating a fold in the Hugoniot curve.

At the end of this procedure, we have completed the calculation of the quantities $\tilde{v}^{SCF}$, $\tilde{u}^+$, $\tilde{Q}^+$ with possibly several values of the quantity S_w^+, corresponding to a given value for T^-, S_w^- and $T^+ \neq T^-$. If we plot all values of S_w^+ for T^+ in the range of temperatures of interest, we obtain the non-isothermal branch of the Hugoniot curve.

Examples of non-isothermal Hugoniot curves are shown in Fig. 3.1.

3.3.2. *Isothermal solution of the Rankine-Hugoniot system.* When we substitute $T^+ = T^-$ into Eq. (3.14) we obtain the simple equation $\Lambda^+\widetilde{Q}^+ = 0$. Therefore $\widetilde{Q}^+ = 0$. Hence we obtain from (3.13) that $\tilde{u}^+ = 1$. Setting $T^+ = T^-$, in addition to $\widetilde{Q}^+ = 0$, $\tilde{u}^+ = 1$ in Eqs. (3.1), (3.2), and (3.3) we obtain the equivalent forms of the Rankine-Hugoniot condition for the Buckley-Leverett equation with no condensation:

$$\left(S_w^+ - S_w^-\right)\tilde{v}^{BL} = f_w^+ - f_w^-, \qquad \left(S_g^+ - S_g^-\right)\tilde{v}^{BL} = f_g^+ - f_g^-. \tag{3.20}$$

This equation shows that for $T^+ = T^-$, any (T^+, S^+) lies in the RH locus of (T^-, S_w^-). For a given S_w^+, Eq. (3.20) furnishes $\tilde{v}^{BL}$. We call this the isothermal or "Buckley-Leverett" branch of the Hugoniot curve; obviously, it does not involve condensation and it contains (T^-, S_w^-).

Remark 3.5. The state (T^-, S_w^-) is also contained in the Hugoniot branch that describes the steam condensation front. As we see in Fig. 3.1 by drawing the isothermal branch as a vertical line through each point (T^-, S_w^-), besides intersecting at this point these two branches often intersect at another one. In examples I-IV in this figure, there are two intersections.

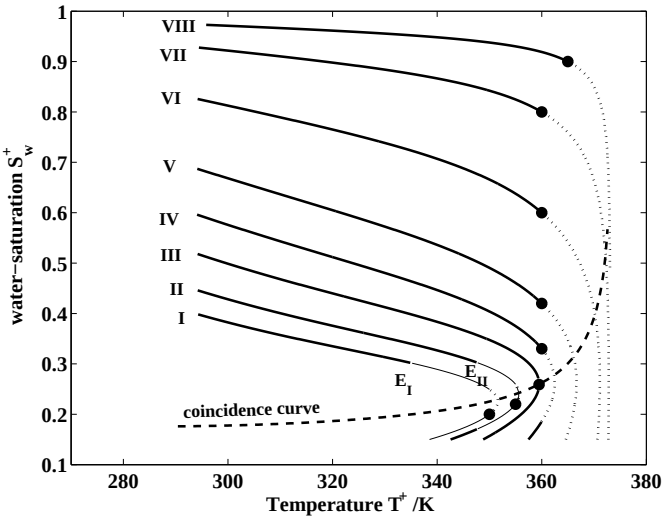

FIGURE 3.1. Hugoniot curves for $(-)$ states (T^-, S_w^-), represented by solid circles with I $= (350, 0.2)$, II $= (355, 0.22)$, III $= (359.5, 0.259)$, IV $= (360, 0.33)$, V $= (360, 0.42)$, VI$=(360, 0.6)$, VII$=(360, 0.8)$, VIII$=(365, 0.9)$. We also show the coincidence curve (dashed). The dotted parts are inadmissible because they correspond to evaporation. The thin parts are inadmissible because they violate the entropy condition (3.23). The thick parts are the admissible $(+)$ states of the steam condensation front.

3.3.3. *The coincidence curve.* If the isothermal and thermal Hugoniot branches intersect twice for a given temperature, we can change the $(-)$ saturation and bring the intersection points together without changing the temperature. This is shown in example III of Fig. 3.1. The set of points generated in this way is called the *coincidence curve*, also displayed in this figure.

Notice that there is no coincidence curve for temperatures exceeding the boiling temperature of water at the prevailing pressure. This is so because as the $(-)$ temperature increases to the boiling temperature, there will be only one intersection for the Hugoniot branches (the $(-)$ state). Examples V - VIII show only one intersection for a vertical line through (T^-, S_w^-).

3.4. **Admissible parts of the Hugoniot curve.** For a given $(-)$ state, in general not all points in the Hugoniot curve represent actual shocks. For instance if characteristics emanate from the shock rather than impinge on it. This would for instance occur in a Buckley-Leverett problem if we would try a solution consisting of a rarefaction, a constant state, a shock and a constant state as opposed to a rarefaction, a shock and a constant state. In this case we consider the following. When $T^+ = T^-$, we have, according to Eq. (3.7), that $v^{SCF} = \lambda^{TH}$. For instance, $(+)$ states near the $(-)$ state such that $v^{SCF} > \lambda^{TH}(-)$ are good approximations to states on a rarefaction curve [19]. (Equation (3.7) defines λ^{TH}). In our case, this rarefaction curve represents evaporation rather than condensation waves, because it has temperatures T^+ exceeding T^-, see the dotted parts of I, II and IV in Fig. 3.1. For this reason, the part of the Hugoniot curve with $T^+ > T^-$ is inadmissible.

The following Lax entropy condition must also be satisfied:

$$\tilde{v}^{SCF} < \tilde{\lambda}^{BL}(+), \tag{3.21}$$

where $\tilde{\lambda}^{BL}(T)$ is defined by

$$\tilde{\lambda}^{BL}(T) = \frac{\partial f_w}{\partial S_w}(T, S_w). \tag{3.22}$$

If there are two solutions satisfying the Hugoniot conditions (3.1), (3.2), (3.3), (3.4), it turns out that only one of them satisfies (3.21). One can verify that in our case the other Lax entropy inequality condition for admissibility is violated. Namely, the following is violated sometimes:

$$\tilde{v}^{SCF} < \tilde{\lambda}^{BL}(-). \tag{3.23}$$

3.4.1. *Examples of non-isothermal Hugoniot curves.* In Fig. 3.1 we show Hugoniot curves for eight different $(-)$ states (indicated by solid circles.) The Hugoniot curves are not drawn below the connate water saturation $S_w = S_{wc}$ because such states are inaccessible under normal flow.

Many non-isothermal Hugoniot curves have a *fold point*, a point where they have a vertical tangent in a (T, S) plane; one can show that (T^-, S_w^-) is a fold point if and only if it belongs to the coincidence curve.

Upstream states in the thin parts of the curve have the additional property that the steam condensation front velocity is larger than the saturation wave velocity and do not satisfy the entropy condition (3.23). That is, they do not lead to admissible solutions, as it is well explained elsewhere [32].

States E on the Hugoniot curve which satisfy the entropy condition marginally i.e., those satisfying the following entropy equality will be shown to have important role in Riemann solutions:

$$\tilde{v}^{SCF} = \tilde{\lambda}^{BL}(-). \tag{3.24}$$

One can prove that points E tends to points $(-)$ as the latter tends to the coincidence curve. Thus, for points $(-)$ on or above the coincidence curve, the inadmissible part of the Hugoniot curve from $(-)$ to E disappears. This is considered the most important feature of the coincidence curve.

4. Non-condensation elementary waves

Considering Gibbs's phase rule and the constant pressure conditions there are two degrees of freedom for single phase gas flow (temperature, composition) and one degree of freedom (temperature) when two phases are present. From the hydrodynamic point of view the saturation is an additional degree of freedom.

4.1. **Two-phase flow.** As discussed in Section 2.3.2, if the temperature changes there is a non-zero source term. Self-similar solutions in this case are shock waves (the steam condensation fronts are studied in another section) or rarefaction waves, which correspond to evaporation, so they are not studied in this work.

If the temperature does not change, all concentrations are constant and the flow reduces to the classical two-phase Buckley-Leverett problem with a gas phase of constant composition.

The isothermal Buckley-Leverett flow admits shocks, rarefactions, or rarefaction-shocks. The shock speed is $v^{BL} = (\varphi/u)\tilde{v}^{BL}$, where v^{BL} was already defined in Eq. (3.20). The (scaled) rarefaction speed was already defined in Eq. (3.22).

4.2. **Hot isothermal gas-water shocks.** We describe shocks that separate regions with two-phase flow from regions with single phase liquid flow, both at high temperature. Such *hot isothermal gas-water (higw)* shocks are a limiting case of two-phase flow, so they have to occur at constant temperature as explained before. Their speed is

$$v^{higw} := \frac{u}{\varphi}\frac{f_w^- - 1}{S_w^- - 1} = \frac{u}{\varphi}\frac{f_g^-}{S_g^-}, \quad \widetilde{v}^{higw} = \frac{f_g^-}{S_g^-}. \tag{4.1}$$

4.3. **Single phase liquid flow.** An accurate description of this flow can be found in [6]. For simplicity, we describe liquid flow under the good approximation that thermal expansivity of water is negligible (the same is true for rock). Thus, the balance equations (2.14), (2.16), (2.18) reduce to

$$\varphi\frac{\partial}{\partial t}\rho_W + \frac{\partial}{\partial x}(u\rho_W) = 0, \tag{4.2}$$

$$\frac{\partial}{\partial t}(H_r + \varphi H_W) + \frac{\partial}{\partial x}(uH_W) = 0. \tag{4.3}$$

Based on (4.2), one can show that $\partial u/\partial x = 0$. We also ignore the temperature dependence of the water and rock heat capacities per unit volume C_W, C_r and disregard liquid water and rock expansivity, so that the wave of interest in the water becomes a thermal contact discontinuity [6]. (This follows from Eq. (4.3).)

Typically this wave exists as a *cooling discontinuity* between hot water with temperature T and water at initial reservoir saturation with temperature T^0; its speed can be written as

$$v^{TH} = u\frac{C_W}{C_r + \varphi C_W}, \quad \widetilde{v}^{TH} \equiv \frac{\varphi}{u}v^{TH}. \tag{4.4}$$

On the other hand, we have verified numerically that in the condensation Hugoniot curve the following inequality is always satisfied for a sequence of states $(-)$, $(+)$, I:

$$\tilde{v}^{SCF}(-,+) \geq \tilde{v}^{TH}(+,I), \tag{4.5}$$

where I denotes the initial state.

5. Determination of the structure of the Riemann solutions

Speed equality of different waves typically represents resonance and generates bifurcations. Hence the loci where such equalities occur are called *bifurcation loci*. If they are curves, they are called *bifurcation curves*.

Whenever a solution path crosses a bifurcation curve, locally the Riemann solution becomes qualitatively different. When a solution path crosses the same set of curves the overall qualitative behavior will be similar. Therefore it is important to study the bifurcation curves.

5.1. **The Hugoniot barrier.** It is possible to show that there is at most one condensation front. Whether there is one or none depends on the injection conditions. When there is no condensation front the downstream liquid region is separated from the upstream two-phase region by an isothermal wave, the *Hot Isothermal Steam Water (hisw) shock* described in Section 4.2. (Our upstream conditions are always two phase and we are excluding evaporation. Thus, non-isothermal conditions contradict the absence of a condensation front.

From the inequality (4.5), there is no thermal wave downstream of the steam condensation front. Thus, when there is a condensation front, its downstream temperature is the initial temperature of the reservoir. The upstream (left) temperature T^- is the injection temperature because there is no condensation.

5.1.1. *Presence or absence of a steam condensation front.* In the presence of a steam condensation front it is useful to separate the solution in three parts: two isothermal two-phase regions separated by the steam condensation front. The isothermal parts can be described exactly as the Buckley-Leverett theory of two-phase flow: the solutions consist of constant states, rarefactions and shocks.

Let us consider the case when the SCF speed is so large that it equals the cooling contact discontinuity speed. We expect this bifurcation to represent the boundary between configurations containing either SCF shocks or cooling discontinuities. We will show that the remarkable speed equalities (5.1)–(5.2) hold along this bifurcation curve. Beyond this bifurcation curve the SCF is absent.

This bifurcation was already studied for the case of pure steam injection in [5].

5.1.2. *Speed equalities.* We will consider states $(-)$ and $(+)$ related by RH conditions for which the total amount of mass transfer and of heat generated is zero. We set $\widetilde{Q}^+$ to zero in Eqs. (3.17) and (3.18); From the first one we obtain the first of the equalities in (5.1). The second one follows from (3.18) and from Remark B.1:

$$\tilde{v}^{SCF} = \frac{f_g^-}{S_g^-} = \frac{\Delta J_H^{-,+}}{\Delta H_m^{-,+}}. \tag{5.1}$$

Taking the limit as $T^+ \to T^-$ into (5.1), we see that (T^-, S_w^-) satisfy the following equation in (T, S) space (see Eqs. (3.16) and (2.19)):

$$\frac{f_g^-}{S_g^-} = \widetilde{\lambda}_o^{TH}(-). \tag{5.2}$$

We see that the $(-)$ states of SCF with $Q^+ = 0$ belong to the locus defined by Eq. (5.2).

We obtain $\tilde{u}^+$ from Eq. (3.13) setting $\widetilde{Q}^+ = 0$. We replace $\tilde{v}^{SCF}$ using the first equality (5.1) into Eq. (3.10). We see that S_g^+ satisfies

$$\frac{u^+}{u^-}\frac{f_g^+}{S_g^+} = \tilde{v}^{SCF}. \tag{5.3}$$

Eqs. (5.2) and (5.3) are the same as $u^+ f_g^+ - \varphi v^{SCF} S_g^+ = 0$, $u^- f_g^- - \varphi v^{SCF} S_g^- = 0$. Hence the $(+)$ state also belongs to the locus (5.2). Thus all Hugoniot curves starting on the locus (5.2) belong to the locus (5.2). Two consequences can be drawn from this fact. First, no Hugoniot curve can cross the locus (5.2), so we call it the *Hugoniot barrier*. The second consequence follows from taking the limits of the $(+)$ and $(-)$ states on the Hugoniot barrier

as they approach each other: thermal rarefaction curves with $q = 0$ also belong to the Hugoniot barrier. Therefore thermal rarefaction curves do not cross the barrier.

We have found a curve in (T, S) space for which the cumulative condensation Q^+ is zero. This curve acts as a barrier for thermal Hugoniot curves. Along it $\widetilde{v}^{SCF}$ equals f_g/S_g both upstream and downstream.

Conversely, first consider a thermal shock with speed $\tilde{v}^{SCF} = f_g^-/S_g^-$. Using this equality into (3.17) we see that $Q^+ = 0$. So the thermal shock belongs to the Hugoniot barrier. Second, consider a thermal shock with speed $\tilde{v}^{SCF} = \Delta J_H^{-,+}/\Delta H_m^{-,+}$. Using this equality into (3.14) we see that $Q^+ = 0$. So again the thermal shock belongs to the Hugoniot barrier. Third, assume the equality of f_g^-/S_g^-, and $\Delta J_H^{-,+}/\Delta H_m^{-,+}$. This condition gives $f_g^- = \alpha S_g^-$ and $\Delta J_H^{-,+} = \alpha \Delta H_m^{-,+}$ with $\alpha > 0$. Substitution into Eq. (3.18) leads to $\widetilde{v}^{SCF} = f_g^-/S_g^- = \Delta J_H^{-,+}/\Delta H_m^{-,+}$. Based on these two facts and Eq. (3.18), we conclude that the equality of any two of the three quantities $\widetilde{v}^{SCF}$, f_g^-/S_g^-, and $\Delta J_H^{-,+}/\Delta H_m^{-,+}$ implies that we are on the Hugoniot barrier.

5.2. **Bifurcation curves involving a steam condensation front.** In Section 5.1 the solutions did not contain a steam condensation front. Here we study bifurcation curves for solutions that contain a steam condensation front.

5.2.1. *The entropy curve.* Given the injection saturation and temperature T^- and the initial temperature T^+ both S_w^- and S_w^+ need to be determined to define the steam condensation front completely. For this reason it is very useful to construct the following *entropy* curve, which represents (T^+, S_w^-) values for which the SCF between (T^-, S_w^-) and (T^+, S_w^+) has its speed v^{SCF} coinciding with the Buckley-Leverett speed at the $(-)$ state. This curve is obtained by substituting Eq. (3.24) into (3.18), obtaining an explicit formula for S_g^-. It is easy to verify that this curve always intersects the coincidence curve at (T^-, S_w^-).

In Figure 6.1 this curve is drawn for $T^- = 360K$. The entropy curve is almost superimposed on the coincidence curve for our example. The reason is that both curves satisfy the condition (3.24) and for the low water saturations involved small changes in the upstream water saturation have a large effect on the saturation wave velocity. So even if the steam condensation front velocities for the full solution curve and the coincidence curve are very different a small saturation change will be able to compensate for this effect.

5.2.2. *The Welge curve.* This bifurcation is determined by the Welge tangency condition if the initial water saturation is $S_w = 1$. It reads

$$\frac{\partial f_w}{\partial S_w} = \frac{1 - f_w}{1 - S_w}. \tag{5.4}$$

The common value of the equality (5.4) is the Welge speed $\tilde{v}^{WELGE}$.

Remark 5.1. Another consequence of the speed equalities in Section 5.1.2 is that if the state $(-)$ lies on the Hugoniot barrier, then taking the limit as $T^+ \to T^-$ in (5.1) leads to

$$\lambda^{TH}(-) = \lim_{T^+ \to T^-} \tilde{v}^{SCF} = \lim_{T^+ \to T^-} \frac{\Delta J_H^{-,+}}{\Delta H_m^{-,+}} = \widetilde{\lambda}_o^{TH}(-). \tag{5.5}$$

Thus we see that the geometric possibility of isothermal rarefaction wave preceding an infinitesimal SCF changes at the Hugoniot barrier.

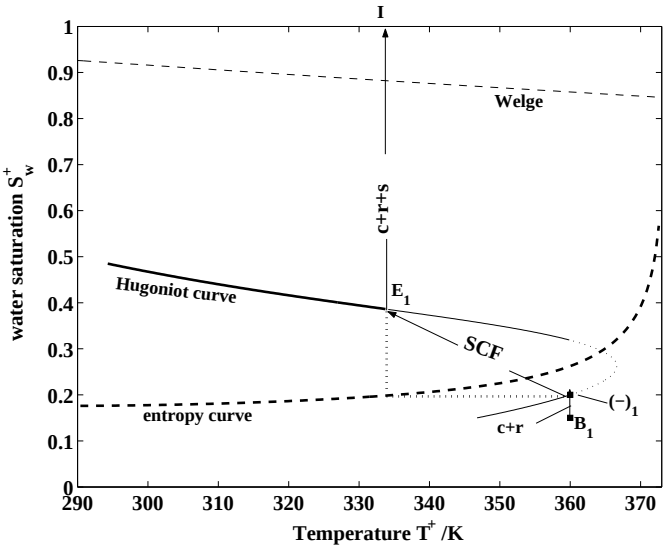

FIGURE 6.1. Construction of solution for injection conditions $B_1 = (T^-, S_w^-) = (360, S_{wc}^-)$. The upstream (left) Buckley-Leverett part of the solution is drawn between the injection point and and consists of a rarefaction part until the steam condensation front is reached. (If the injection saturation is above the connate water saturation a constant state precedes the rarefaction part.) From B_1 to E_1 of the Hugoniot curve there is a shock also called the steam condensation front. Finally the curve follows the downstream Buckley-Leverett part from to the initial condition $I = (T^{ini}, S_w^{ini}) = (335.1, 1.0)$. The other lines are discussed in the text.

Remark 5.2. Equating v^{SCF} from the two equations (5.1), (5.3) we see that along the Hugoniot barrier the following equality holds:

$$\frac{u^+}{u^-} = \frac{S_g^+}{f_g^+}\frac{f_g^-}{S_g^-}.$$

6. Riemann solution for an initially water-saturated core

Remark 6.1. With fixed T^-, as S_g^- decreases to zero, $\tilde{v}^{SCF}$ increases to the speed of the thermal wave in the pure liquid, $\tilde{\lambda}^{TH}$; this fact follows from the convexity of $\rho_{gw}(T)$. It is useful for the first, second, and third cases.

6.1. **First case.**

We claim that for very low water saturation at the injection point, we have:

$$\tilde{v}^{SCF} > \tilde{\lambda}^{BL}(-). \tag{6.1}$$

(This follows from the fact that at $S_w^- = S_{wc}$, we have $\tilde{\lambda}^{BL}(-) = \frac{\partial f_w}{\partial S_w}(S_{wc}) = 0$, while $\tilde{v}^{SCF} > 0$). Eq. (6.1) for the injection saturation defines the first case. The initial condition denoted as I in Figure (6.1), which defines the initial saturation $S_w = 1$ and the initial temperature T^{ini} (in our example we choose $T^{ini} = 335.1K$). It can be shown that the downstream (right) shock temperature $T^+ = T^{ini}$.

First we draw the entropy curve associated with the given injection temperature T^{inj} (here $T^{inj} = 360\ K$). It has been shown above that $T^{inj} = T^-$, the upstream (left) shock

temperature. Now we want to determine the saturation of the upstream (left) shock state $(-)_1$. We draw a vertical line through I. The intersection of this line with the entropy curve determines the saturation S_w^-. A horizontal line transports this saturation value to determine the state $(-)_1 = (T^-, S_w^-)$. In our example $(T^-, S_w^-) = (360, 0.2)$. The first case requires that the injection saturation satisfies $S_w^{inj} < S_w^-$. Indeed S_w^- satisfies all Hugoniot conditions and the entropy tangency condition (5.4). The Hugoniot curve starting at state $(-)_1$ intersects the vertical line at the state E_1. Upstream of point $(-)_1$ we have isothermal conditions and we can apply the classical Buckley-Leverett theory.

The solution (see Figure 6.1) is a wave sequence consisting of a constant state, a rarefaction part at T^{inj} and subsequently the steam condensation front. Downstream of the steam condensation front there will be the constant state E_1, followed by a Buckley-Leverett rarefaction and shock up to the state I. All of this is indicated by the path $B_1 \xrightarrow{c+r} (-)_1 \xrightarrow{SCF} E_1 \xrightarrow{c+r+s} I$. If the injection saturation is equal to the connate water saturation the path $B_1 \to (-)_1$ has no constant state.

Downstream of the SCF, i.e., in $E_1 \xrightarrow{c+r+s} I$ there is a constant state followed by a Buckley-Leverett rarefaction wave until we attain the *cold isothermal gas-water shock (cigw)* with speed

$$v^{cigw} = \frac{u^o}{\varphi}\left(\frac{f_g}{S_g}\right)_{T^0}, \widetilde{v}^{cigw} = \frac{u^o}{u^-}\left(\frac{f_g}{S_g}\right)_{T^0}, \tag{6.2}$$

to the initial state where the gas saturation goes to zero. This cigw shock appears in cases one to three.

The separation between the first and second cases is the coincidence locus described in Section 5.2.1.

6.2. **Second case.** The water saturation at the injection point is high enough so that the velocity of the steam condensation front satisfies the following inequalities for $\tilde{v}^{WELGE}$ defined in Equation (5.4)

$$\tilde{v}^{WELGE} \leq \tilde{v}^{SCF} \leq \tilde{\lambda}^{BL}(-). \tag{6.3}$$

Figure 6.2 shows a number of cases that differ in the left state only as to the injection saturation. In all of these cases there is a constant state from the injection condition indicated by B to the left point $(-)$ (just upstream) of the steam condensation front. (Of course, B and $(-)$ coincide.) In Case 2, the left state $(-)_1$ lies below the entropy curve. (This means that part of the Hugoniot curve does not represent admissible solutions and hence it is represented by a thin line). For Case 2 the solution path (or wave sequence) typically is $B_2 \xrightarrow{c} (-)_2 \xrightarrow{SCF} (+)_2 \xrightarrow{c+r+s} I$. Case 2 comprises all solutions with Hugoniot curves such as the ones belonging to B_2, starting below the coincidence curve, and to B_3, starting above the coincidence curve. All solutions for this case, which do not intersect the *Welge* curve to the right of the vertical straight line, follow the same pattern.

These solutions have a constant state $B \xrightarrow{c} (-)$, the steam condensation front $(-) \xrightarrow{SCF} (+)$, a constant state, a rarefaction and a shock to the initial state I, $(+) \xrightarrow{c+r+s} I$.

The second and third cases are separated by the Welge curve described in Section 5.2.2.

6.3. **Third case.** Figure 6.2 shows also the case with Hugoniot curves, such as the one belonging to B_4, that do intersect the *Welge* curve left of B and to the right of the vertical straight line. Because we crossed the *Welge* curve a bifurcation has occurred. Indeed for

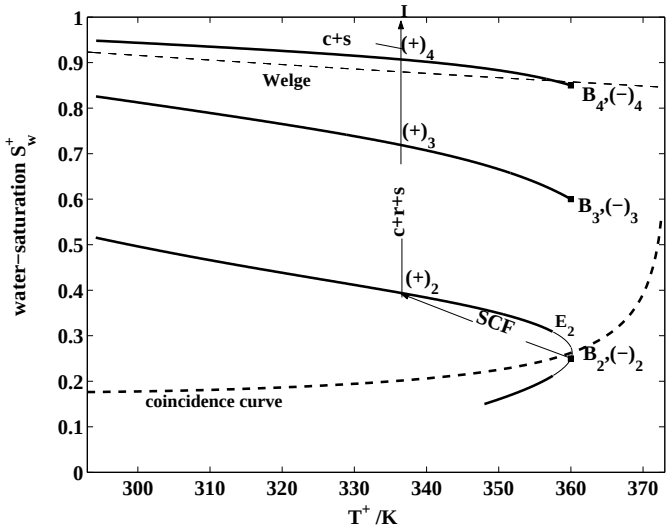

FIGURE 6.2. Construction of solution for injection conditions $B_2 = (T^-, S_w^-) = (360, 0.25)$, $B_3 = (T^-, S_w^-) = (360, 0.6)$, $B_4 = (T^-, S_w^-) = (360, 0.85)$ represented by solid circles. There is a constant state between the injection condition and the left state of the steam condensation front (SCF) denoted by $(-)_2$. The SCF is from $(-)_2$ to $(+)_2$, i.e. the right state of the SCF. For the initial condition I there follows a constant state, a rarefaction and a shock.

$(+)_4 \rightarrow I$ the rarefaction disappeared as can be easily verified from a classical Buckley-Leverett construction using fractional flow curves. The complete wave sequence is a constant state $B \xrightarrow{c} (-)$, then the steam condensation front $(-) \xrightarrow{SCF} (+)$, a constant state and finally a shock to the initial condition I, $(+) \xrightarrow{c+s} I$.

Figure 6.3 shows two examples of injections also representative of Case 3, with very high water saturations with solutions starting at B_5, B_6. The *Welge* curve is not visible because it is well below $S_w = 0.97$. The solution path for injection conditions B_5 is given by $B_5 \xrightarrow{c} (-)_5 \xrightarrow{SCF} (+)_5 \xrightarrow{c+s} I$. It is analogous for B_6.

The third and fourth cases are separated by the Hugoniot barrier described in Section 5.1.

6.4. **Fourth case.** The water saturation at the injection point is so high that at the injection temperature the isothermal gas-water (higw) shock speed satisfies

$$\widetilde{v}^{higw}(-) \leq \widetilde{\lambda}^{TH}(-). \tag{6.4}$$

If the inequality (6.4) is satisfied we will have no steam condensing at the front where the temperature is reduced. Instead we have a higw shock followed by a cooling discontinuity as given by Eq. (4.4). Between the injection point and the front where the temperature is reduced now there is a hot two phase zone and a hot single phase zone.

An example of the fourth case is the solution with initial condition B_7 is on the other side of the Hugoniot barrier curve. (See Figure 6.3.) This means that the Buckley-Leverett gas-water shock is slower than the speed of a temperature wave carried by pure liquid water so there is no steam condensation front. The solution path is $B_7 \xrightarrow{c} (-)_7 \xrightarrow{s} () \xrightarrow{cool} I$.

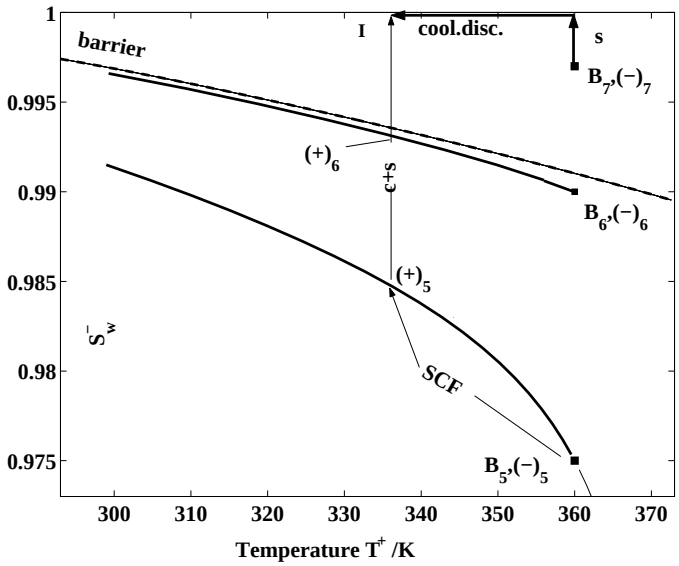

FIGURE 6.3. Construction of solution for injection conditions $B_5 = (T^-, S_w^-) = (360, 0.975)$, $B_6 = (T^-, S_w^-) = (360, 0.99)$, $B_7 = (T^-, S_w^-) = (360, 0.997)$. The curves B_5, B_6 start and remain below the *barrier* curve. For B_5, B_6 there are a constant state, the steam condensation front, a constant state and a shock to I. For B_7 we have a constant state, a hot isothermal gas water shock and a thermal contact discontinuity to I.

In this case there will be a shock from $(-)_7$ following the vertical arrow also called the *hot isothermal gas-water* shock and a horizontal arrow representing the cooling discontinuity.

7. Conclusions

1. A method is presented with which all qualitatively different solutions can be found. A bifurcation, i.e. a qualitatively different solution, can occur when the solution crosses bifurcation loci (where wave velocities become equal).
2. For an initial state where the porous medium is fully saturated with water four different types of solutions are found, depending on the injection conditions. This general pattern is independent of realistic variations of the physical quantities.
3. Three of these solutions contain a cold gaseous zone downstream of the steam condensation front. Such a zone is considered a prerequisite for the avoiding downward movement of the pollutants (DNAPL's).
4. The fourth solution, for which the gas saturation disappears upstream of the temperature wave, only occurs for impractical injection conditions. Moreover, the presence of injected nitrogen greatly reduces the region in phase space where there is no steam condensation front. This region corresponds to less than 0.01 nitrogen saturation, as shown in Fig. 6.3.

Acknowledgments: This work was partially done at IMA, University of Minnesota, and therefore partially funded by NSF. We also thank Beata Gundelach for careful and expert typesetting of this paper.

References

[1] BEEK, W.J. AND MUTZALL, M.K., *Transport ohenomena,* John Wiley & Sons (1975), ISBN 0-471-06174-5

[2] BETZ, C., FARBAR, A., and SCHMIDT, R., *Removing volatile and semi-volatile contaminants from the unsaturated zone by injection of a steam air mixture.* Contaminated Soil. Thomas Telford, London, pp 575-584 (1998)

[3] BIRD, R.B., STEWART, W.E., and LIGHTFOOT, E.N., *Transport Phenomena*, John Wiley & Sons (1960), ISBN 0-471-07392 X .

[4] BROOKS, R.H., and COREY, A.T., *Properties of porous media affecting fluid flow*, J. Irr. Drain. Div., Proc., Am. Soc. Civ. Eng. June (1966), 61-88.

[5] BRUINING, J., and DUIJN, C.J., *Uniqueness conditions in a hyperbolic model for oil recovery by steamdrive*, Computational Geosciences **4**, 65-98 (2000).

[6] BRUINING, J., MARCHESIN, D., and DUIJN, C.J., *Steam injection into water-saturated porous rock*, Computational and Applied Mathematics, accepted, 2003, and IMPA preprint no. 136/2002, 2002.

[7] COATS, K. H., *In-situ combustion model*, Soc. Pet. Eng. J., Dec. 1980, pp. 533–554.

[8] COATS, K.H.,THOMAS, L.K. AND PIERSON, R.G., *Compositional and black oil simulation,* SPE Reservoir Evaluation & Engineering, August 1998, 372-379 (see also ABDALLA, A, A AND COATS, K.H., *Three-Phase, Experimental and Numerical Simulation Study of the Steam Flood Process,* (1971), 46th Annual Fall Meeting of the Society of Petroleum Engineers of AIME, to be held in New Orleans, La., Oct. 3-6, SPE 3600)

[9] DAKE, L.P., *Fundamentals of reservoir engineering*, Elsevier Science Publishers, Amsterdam, 1978.

[10] DULLIEN, F.A.L., *Porous media; fluid transport and pore structure*, Academic Press, N.Y. (1979).

[11] DYKE, M. VAN., *Perturbation Methods in Fluid Mechanics*, chapter 5, The Parabolic Press, Stanford, 1975.

[12] GODDERIJ, R.R.G.G., BRUINING, J. AND MOLENAAR, J, *A fast 3D interface simulator for steamdrives*, SPE Journal 4 (4), December (1999), 400-408

[13] HO, C.K., and UDELL, K.S., *An experimental investigation of air venting of volatile liquid hydrocarbon mixtures from homogeneous and heteroheneous media.* Journal of Contaminant Hydrology **11** 291-316 (1992)

[14] HUNT, J.R., SITAR, N, and UDELL, K.S.., *Non-aqueous phase liquid transport and clean up: Part I, Analysis of Mechanisms.* Water Resources Research **24** (8) 1247-1258 (1988)

[15] HUNT, J.R., SITAR, N, and UDELL, K.S.., *Non-aqueous phase liquid transport and clean up: Part II, Experimental studies.* Water Resources Research **24** (8) 1259-1269 (1988)

[16] KASLUSKY, S.F. and UDELL, K.S.., *A theoretical model of air and steam co-injection to prevent the downward migration of the DNAPL's during steam enhanced extraction.* Journal of Contaminant Hydrology **55** 213-232 (2002)

[17] BUCKLEY, S.E., and LEVERETT, M.C., *Mechanism of fluid displacement in sands*, Trans. AIME, pp.107-116, 1941.

[18] MANDL, G., and VOLEK, C.W., *Heat and mass transport in steamdrive processes*, Soc. Pet. Eng. J., (1969) 57-79.

[19] MARCHESIN, D. AND PLOHR, B., *Wave structure in WAG recovery,* SPEJ **6**(2) 209-219 (2001), SPE71314

[20] MARLE, C.M., *On macroscopic equations governing multiphase flow with diffusion and chemical reactions in porous media,* Int. J. Engng. Sci., **20**, 5, 643-662 (1982)

[21] OLEĬNIK, O., *On the uniqueness of the generalized solution of the Cauchy problem for a non-linear system of equations occuring in mechanics*, Uspekhi Mat. Nauk. **12**, 169–176, 1957.

[22] POPE, G.A., *The application of fractional flow theory to enhanced oil recovery*, Soc. Pet. Eng. J., **20** (1980) 191-205.

[23] RATHFELDER, K., YEH, W.W.-G, and MACKAY, D., *Mathematical simulation of soil vapor extraction systems: model development and numerical examples.* Journal of Contaminant Hydrology **8** 263-297 (1991)

[24] SCHMIDT, R., GUDBJERG, J., SONNENBORG, T.O. and JENSEN, K.H., *Removal of NAPL's from the unsaturated zone using steam: prevention of downsward migration by injecting mixtures of steam and air.* Journal of Contaminant Hydrology **55** 233-260 (2002)

[25] SCHMIDT, R., BETZ, C., and FAERBER, A., *LNAPL and DNAPL behaviour during steam injection into the unsaturated zone.* International Association of Hydrological Sciences Publication **250**, 11-117 (1998)
[26] SHUTLER, N.D., *A one dimensional analytical technique for predicting oil recovery by steam flooding*, Soc. Pet. Eng. J., (1972) 489-498.
[27] SMOLLER, J., *Shock Waves and Reaction-Diffusion Equations*, Springer-Verlag, New York (1980).
[28] STEWART, L.D. and UDELL, K.S., *Mechanisms of residual oil displacement by steam injection*, SPE Reservoir Engineering, (November-1988) 1233-1242.
[29] TORTIKE, W.S., and FAROUQ ALI, S.M., *Saturated-steam-property functional correlations for fully implicit reservoir simulation*, SPERE (November 1989) 471-474.
[30] WEAST, R.C., *CRC Handbook of Chemistry and Physics*, 58^{th} edition, CRC Press, Inc. 1977-1978.
[31] WINGARD, J.S. and ORR, F.M., *An analytical solution for steam/oil/water displacements*, SPE Advanced Technology Series, **2** (1994) 167-176.
[32] WITHAM, G.B., *Linear and Nonlinear Waves*, John Wiley and Sons, NY, 1974.
[33] YORTSOS, Y.C., *Distribution of fluid phases within the steam zone in steam injection processes*, Soc. Pet. Eng. J., (1984) 458-466.

Appendix A. Physical quantities; symbols and values

In this Appendix we summarize the values and units of the various quantities used in the computation and empirical expressions for the various parameter functions. For convenience we express the heat capacity of the rock C_r^p in terms of energy per unit volume of *porous medium* per unit temperature *i.e.* the factor $1-\varphi$ is already included in the rock density. All other densities, concentrations are expressed in terms of mass per unit volume of the phase. All enthalpies per unit mass are with respect to the enthapies at the reference temperature of the components in their standard form. All heat capacities are at constant pressure. All enthapies per unit mass are zero for the component in its standard form at the reference temperature.

Table A. Summary of physical input parameters and variables

Physical quantity	*Symbol*	*Value*	*Unit*
Heat capacities per unit mass	$c_W,\ c_{gW}, c_{gN}$	$\frac{dh_W}{dT}, \frac{dh^s_{gW}}{dT}, \frac{dh_{gN}}{dT}$	[J/(kgK)]
Water heat capacity	C_W	dH_W/dT	[J/(m^{3}K)]
Steam, N_2 heat capacity	C_{gW}, C_{gN}	$\frac{dH^s_{gW}}{dT}, \frac{dH_{gN}}{dT}$	[J/(m^{3}K)]
Effective rock heat capacity	C_r	2.029×10^6	[J/(m^{3}K)]
Water, steam fractional functions	f_w, f_g	Eq. (2.2).	[m^3/m^3]
Steam/N_2 enthalpy per unit mass	h_{gW}, h_{gN}	Eq. $A.3, A.4$	[J/kg]
Steam/N_2 enthalpy	H_{gW}	$\rho_{gW}(T)h_{gW}(T)$	[J/m^3]
	H_{gN}	$\rho_{gN}(T)h_{gN}(T)$	[J/m^3]
Partial steam/N_2 enthalpy	H_{gw}	$\rho_{gw}(T)h_{gW}(T)$	[J/m^3]
	H_{gn}	$\rho_{gn}(T)h_{gN}(T)$	[J/m^3]
Rock enthalpy	H_r	$C_r(T-\bar{T})$	[J/m^3]
Water enthalpy	H_W	$\rho_W(T)h_W(T)$	[J/m^3]
Porous rock permeability	k	1.0×10^{-12}	[m^2]
Water, steam relative permeabilities	k_{rw}, k_{rg}	Eq. (A.11) .	[m^3/m^3]
Pressure	p_{tot}	1.0135×10^5	[Pa]
Mass condensation rate	$q_{g\to a,w}$	Eq. 2.1	[kg /(m^{3}s)]
Cumulative mass condensation	Q	Eq. (2.17).	[kg /m^3]
Water, steam saturations	S_w, S_g	Dependent variables.	[m^3/m^3]
Connate water saturation	S_{wc}	0.15	[m^3/m^3]
Water injection saturation	S_w^{inj}		[m^3/m^3]
Temperature	T	Dependent variable.	[K]
Reservoir temperature	T^{ini}	293.	[K]
Injection temperature	T^{inj}	$293 - 373.$	[K]
Water, steam phase velocity	u_w, u_g	Eq. (2.3).	[m^3/(m^{2}s)]
Total Darcy velocity	u	$u_w + u_g$.	[m^3/(m^{2}s)]
Total injection velocity	u^{inj}	$u_w^{inj} + u_g^{inj}$.	[m^3/(m^{2}s)]
SCF velocity	v^{SCF}	.	[m/s]
Water, steam viscosity	$\mu_w,\ \mu_g$	Eq. (A.6), Eq. (A.7).	[Pa s]
Steam, nitrogen concentrations	$\rho_{gw},\ \rho_{gn}$	Eq. (A.9)	[kg/m^3]
Pure water, steam, nitrogen densities	$\rho_W,\ \rho_{gW}, \rho_{gN}$	1000,Eqs.(2.8) .	[kg/m^3]
Rock porosity	φ	0.38	[m^3/m^3]
Water evaporation heat	$\bar{\Lambda}$	Eq. (2.12),(A.5).	[J/kg]

A.1. **Temperature dependent properties of steam and water.** We use reference [29] to obtain all the temperature dependent properties below. The water and steam densities used to obtain the enthalpies are defined at the bottom. First we obtain the boiling point T^{eq} at the given pressure p, i.e.

$$T^{eq} = 280.034 + \varrho(14.0856 + \varrho(1.38075 + \varrho(-0.101806 + 0.019017\varrho))), \qquad (A.1)$$

where $\varrho = \log(p)$ and p is the pressure in [k Pa]. The evaporation heat [J/kg] is given as a function of the temperature T at which the evaporation occurs. We use atmospheric pressure ($p = 101.325$ [k Pa]) in our computations.

The liquid water enthalpy $h_w(T)$ [J/kg] as a function of temperature is approximated by

$$h_w(T) = 2.36652 \times 10^7 - 3.66232 \times 10^5 T + 2.26952 \times 10^3 T^2 - 7.30365 T^3 + 1.30241 \times 10^{-2} T^4$$
$$-1.22103 \times 10^{-5} T^5 + 4.70878 \times 10^{-9} T^6 - \overline{h}_w. \tag{A.2}$$

The steam enthalpy $h_{gW}[J/kg]$ as a function of temperature is approximated by

$$h_{gW}(T) = -2.20269 \times 10^7 + 3.65317 \times 10^5 T - 2.25837 \times 10^3 T^2 + 7.3742 T^3$$
$$- 1.33437 \times 10^{-2} T^4 + 1.26913 \times 10^{-5} T^5 - 4.9688 \times 10^{-9} T^6 - \overline{h}_w. \tag{A.3}$$

The nitrogen enthalpy $h_{gN}[J/kg]$ as a function of temperature is approximated by

$$h_{gN}(T) = 975.0 T + 0.0935 T^2 - 0.476 \times 10^{-7} T^3 - \overline{h}_{gN}. \tag{A.4}$$

The enthalpies $h_w(T), h_{gN}(T)$ vanish at a reference temperature $\overline{T} = 293K$. For the latent heat $\Lambda(T)[J/kg]$ or evaporation heat we obtain

$$\Lambda(T) = \left(7.1845 \times 10^{12} + 1.10486 \times 10^{10} T - 8.8405 \times 10^7 T^2 + 1.6256 \times 10^5 T^3 - 121.377 T^4\right)^{\frac{1}{2}}. \tag{A.5}$$

The temperature dependent liquid water viscosity μ_w $[Pas]$ is approximated by

$$\mu_w = -0.0123274 + \frac{27.1038}{T} - \frac{23527.5}{T^2} + \frac{1.01425 \times 10^7}{T^3} - \frac{2.17342 \times 10^9}{T^4} + \frac{1.86935 \times 10^{11}}{T^5}. \tag{A.6}$$

We assume that that the viscosity of the gas is independent of the composition.

$$\mu_g = 1.826\,4 \times 10^{-5} \left(\frac{T}{T^b}\right)^{0.6}. \tag{A.7}$$

The water saturation pressure as a function of temperature is given as

$$p^{sat} = 10^3(-175.776 + 2.29272 T - 0.0113953 T^2 + 0.000026278 T^3$$
$$-0.0000000273726 T^4 + 1.13816 \times 10^{-11} T^5)^2 \tag{A.8}$$

The corresponding concentrations ρ_{gw}, ρ_{gn} are calculated with the ideal gas law

$$\rho_{gw} = \frac{M_W\ p^{sat}}{RT},\ \rho_{gn} = \frac{M_N\ (p^{tot} - p^{sat})}{RT}\ , \tag{A.9}$$

where as the pure phase densities are given in Eqs. (2.8) where the gas constant $R = 8.31[J/mol/K]$

The liquid water density as a function of the temperature $T[K]$ is given as

$$\rho^W(T) = 3786.31 - 37.2487 T + 0.196246 T^2 - 5.04708 \times 10^{-4} T^3$$
$$+6.29368 \times 10^{-7} T^4 - 3.08480 \times 10^{-10} T^5. \tag{A.10}$$

We use, however, $\rho^W(T) = 1000$ in the computations for convenience.

For simplicity the liquid water density is assumed to be constant at $998.2.kg/m^3$

A.2. **Constitutive relations.** The relative permeability functions k_{rw} and k_{rg} are considered to be power functions of their respective saturations [10], i.e.

$$k_{rw} = \begin{cases} k'_{rw}\left(\frac{S_w - S_{wc}}{1-S_{wc}-S_{gr}}\right)^{n_w} \\ 0 \end{cases}, k_{rg} \begin{cases} k'_{rg}\left(\frac{S_g - S_{gr}}{1-S_{wc}-S_{gr}}\right)^{n_g} & \text{for} \quad S_{wc} \le S_w \le 1, \\ 1 & \text{for} \quad S_w < S_{wc}. \end{cases} \tag{A.11}$$

For the computations we take $n_w = 2$ and $n_g = 2$. The end point permeabilities k'_{rw}, k'_{rg} are 0.5 and 0.95 respectively. The connate water saturation S_{wc} is given in the table.

Appendix B. Speed equalities at the Hugoniot barrier

Introducing the following abbreviations

$$\mathcal{C}_W = \rho_W^- \left(h_W^- - h_W^+\right), \quad \mathcal{C}_g^s = \rho_{gw}^-(h_{gW}^{s-} - h_{gW}^{s+}) + \rho_{gn}^-(h_{gN}^- - h_{gN}^+),$$

we obtain for the speed of the cooling discontinuity wave in the water

$$\widetilde{v}^{TH} = \frac{\rho_W^- \left(h_W^- - h_W^+\right)}{\left(H_r^- - H_r^+\right)/\varphi + \rho_W^- \left(h_W^- - h_W^+\right)} = \frac{\mathcal{C}_W}{\mathcal{C}_r/\varphi + \mathcal{C}_W}. \tag{B.1}$$

We use Eq. (3.16)

$$\frac{\Delta J_H^{-,+}}{\Delta H_m^{-,+}} = \frac{\mathcal{C}_W f_w^- + \mathcal{C}_g^s f_g^-}{\mathcal{C}_r/\varphi + \mathcal{C}_W S_w^- + \mathcal{C}_g^s S_g^-}. \tag{B.2}$$

We equate $\widetilde{v}^{TH}$ from Eq. (B.1) and the speed of the hot isothermal gas water shock given by (4.1) and obtain the second equality below

$$\frac{1-f_w^-}{1-S_w^-} = \frac{f_g^-}{S_g^-} = \frac{\mathcal{C}_W}{\mathcal{C}_r/\varphi + \mathcal{C}_W} = \frac{\mathcal{C}_W + \mathcal{C}_g^s f_g^-}{\mathcal{C}_r/\varphi + \mathcal{C}_W + \mathcal{C}_g^s S_g^-} = \frac{\mathcal{C}_W f_w^- + \mathcal{C}_g^s f_g^-}{\mathcal{C}_r/\varphi + \mathcal{C}_W S_w^- + \mathcal{C}_g^s S_g^-}.$$

The third equality is obtained by multiplying the second fraction by $\mathcal{C}_g^s$ and adding it to the third fraction. For the fourth equality we multiply the first fraction by $\mathcal{C}_W$, add the fourth fraction and simplify.

Remark B.1. By procedures similar to the one above we reach the following conclusion. Consider the wave speeds: $\frac{f_g^-}{S_g^-}$, $\frac{\Delta J_H^{-,+}}{\Delta H_m^{-,+}}$, and $\widetilde{v}^{TH}$; if any of the two are equal, then the three are equal.

Remark B.2. We show that $T^+ \neq T^-$ implies that $\frac{\rho_{gw}^-}{\rho_{gw}^+} - \frac{\rho_{gn}^-}{\rho_{gn}^+}$ is non-zero. Using Eqs. (2.9), (2.8), and (2.10) we can write

$$\frac{\rho_{gw}^-}{\rho_{gw}^+} - \frac{\rho_{gn}^-}{\rho_{gn}^+} = \frac{T^+}{T^-}\left(\frac{\rho_{gW}^+}{\rho_{gW}^-}\frac{\rho_{gw}^-}{\rho_{gw}^+} - \frac{\rho_{gN}^+}{\rho_{gN}^-}\frac{\rho_{gn}^-}{\rho_{gn}^+}\right) = \frac{T^+}{T^-}\left(\frac{\psi_{gw}^- - \psi_{gw}^+}{\left(1-\psi_{gw}^+\right)\psi_{gw}^+}\right) > 0. \tag{B.3}$$

where we use Figure 2.2 to see that ψ_{gw} is a monotone function of temperature. The final quantity is positive for our case with $T^+ < T^-$.

Dietz Laboratory, Centre of Technical Geoscience, Mijnbouwstraat 120, 2628 RX Delft, The Netherlands
E-mail address: J.Bruining@citg.tudelft.nl

Instituto de Matemática Pura e Aplicada, Estrada Dona Castorina 110, 22460-320 Rio de Janeiro, RJ, Brazil
E-mail address: marchesi@impa.br